

A stochastic model for solar type III bursts

H. Isliker¹, L. Vlahos¹, A.O. Benz², and A. Raoult³

¹ Section of Astrophysics, Astronomy and Mechanics, Department of Physics, University of Thessaloniki, GR-540 06 Thessaloniki, Greece (isliker@astro.auth.gr; vlahos@astro.auth.gr)

² Institute of Astronomy, ETH Zürich, CH-8092 Zürich, Switzerland (benz@astro.phys.ethz.ch)

³ DASOP, UA 324, Observatoire de Paris, Section d' Astrophysique, 5 Place Jules Janssen, F-92195 Meudon Principal Cedex, France (Antoinette.Raoult@obspm.fr)

Received 5 December 1997 / Accepted 20 May 1998

Abstract. A stochastic model for type III bursts is introduced, discussed, and compared to observations. The active region is assumed to be inhomogeneous, with a large number of emerging magnetic fibers. At their bases, random energy release events take place, in the course of which electrons are accelerated, travel along the fibers and eventually undergo the bump-on-tail instability. In the non-linear regime, the formed Langmuir waves induce strong turbulence in the ambient plasma, with secondary electrostatic waves appearing. Wave-wave scattering finally leads to the emission of transverse electro-magnetic waves at the fundamental and the harmonic of the local plasma-frequency. The superposition of the emissions from all the fibers yields a model spectrogram for type III bursts (flux as a function of frequency and time).

Peak-flux distributions of the model are compared to the ones of five observations of type III bursts. It turns out that, in a statistical sense, the model is largely compatible with the observations: the majority of the observations can be considered generated by a process which corresponds with the presented model. The details of the different sub-processes constituting the model play no decisive role concerning the statistical properties of the generated spectrograms, to describe them approximately by randomizing the unknown elements is sufficient. Therewith, the correspondence of the model with the data is not unique. Likewise, intrinsic shortness of observed type III events does not allow a strict enough discrimination between different possible sub-processes of the model through statistical tests.

With that, the conclusion is that the observations are compatible with a model which assumes (i) a randomly structured active region, (ii) a flare-particle acceleration-process which is fragmented into a large number of sub-processes, (iii) a distribution of the accelerated particles which is a random fraction of the ambient density and of power-law form with random index, and (iv) the fragmentary acceleration events to occur randomly in time, i.e. the temporal structure of type III events to be random, without any correlations between the individual bursts.

Key words: acceleration of particles – chaos – waves – methods: data analysis – Sun: flares – Sun: radio radiation

1. Introduction

It is commonly assumed that solar flares are fragmented, being made up by a huge number of small energy-release events in a highly inhomogeneous corona. This conclusion is based on the interpretation of non-thermal flare-emissions in the radio and hard X-ray range: type III and narrow-band radio-spikes spectrograms, as well as hard X-ray time series are full of fine structures in frequency (space) and time (see e.g. Benz and Aschwanden 1991; reviews in van den Oord 1994).

In this paper, we will concentrate on type III events, the signature of electron beams accelerated during the impulsive phase of flares (see e.g. Mc Lean and Labrum, 1985). Type III events reflect the crucial elements of the flare phenomenon, namely 1) the energy release mechanism, 2) the acceleration process of non-thermal particles, 3) their transport along field lines, and 4) the generation of the observable emissions. Moreover, the up to 100 type III bursts (electron beams) during the impulsive phase of flares contain information on the temporal and spatial organization of the flare as a whole, i.e. on the dynamics of the process during its duration of typically one minute, and on its boundary condition, the active region in the corona.

Concerning the explanation of *single* electron beams, many theoretical enquiries as well as a wealth of observations have been undertaken to understand each of the four elements mentioned above, a synthesis is still missing, however (see e.g. Mc Lean and Labrum, 1985; Bastian et al. 1998): The energy in a flare is most likely released by magnetic reconnection in current sheets (see e.g. Priest 1992), and electrons are accelerated by secondary processes (see e.g. Anastasiadis et al. 1997). They afterwards stream along open field lines, and possibly undergo the bump-on-tail instability, creating electro-static waves along their path (e.g. Benz 1993). Whether these waves are driven into a strong or weak turbulent regime is still disputed (see e.g. Cairns & Robinson 1995; Robinson 1997; Papadopoulos 1975). In both approaches, observable radio emission is generated by wave-wave or wave-particle interactions.

Send offprint requests to: H. Isliker

Correspondence to: H. Isliker

Concerning the *global* aspects of flares, regular structures such as periodicities or low-dimensional chaos have been searched for, but not found. What is observed is compatible with randomness (or chaos which is so high-dimensional that in every practical sense it can be considered as randomness; Isliker and Benz 1994, Isliker 1996). The field geometry in the active region is not observable down to the necessary small scales due to angular broadening of the radio-sources by scattering of emissions in the turbulent coronal plasma (Bastian 1994). Models currently under discussion for the active region and its global dynamics are based on the theory of cellular automata and self-organized criticality, assuming therewith stochastic processes in an inhomogeneous and fragmented corona (Lu and Hamilton 1991; Vlahos et al. 1995).

We present a model for solar type III events which bases on the current theory of the behaviour of single electron beams and on the known global properties of flares. The model is of stochastic nature in what concerns the temporal dynamics and the elements which are due to spatial boundary conditions in the active region: we assume that, in the active region, at random times and at random sites electrons are accelerated to a power-law distribution in energy with random index. Every such acceleration takes place at the base of an open fiber (magnetic flux-tube), which carries its own atmosphere. The electrons stream outwards and possibly develop a bump-on-tail-instability which creates a regime of electro-static turbulence, with secondary electro-static waves appearing. In this medium, wave-wave coupling generates observable emission at the fundamental and the harmonic of the local plasma frequency. The superposition of the emissions of the different fibers finally yields a model radio-spectrogram (emitted flux as a function of frequency and time). Throughout in this model, the unknown parameters are represented by random values (in reasonable ranges).

The comparison of the model to observational data will be focused on the global (statistical) properties of type III events, and not on the properties of single electron beams. The question we want to answer is whether the model captures the statistical properties of type III events, although it contains several simplifying assumptions due to the fact that, so far, neither theory has more precise answers to many questions, nor all the parameters are observationally accessible. The statistical quantity we use for a comparison of the model to observations is the probability distribution of the peak fluxes at fixed frequencies.

In Sect. 2 we introduce the type III model, in Sect. 3 the peak-flux distributions of the model spectra and of the observed type III events are presented and compared to each other, and Sect. 4 contains the conclusions.

2. The model

2.1. Overview

The elements of the model, explained below in details, are:

1. *Fragmentation of the active region*: active regions are assumed to be strongly inhomogeneous. Particularly, a large number of fibers (open flux tubes) is assumed to emerge

from the active region. Each fiber has its random characteristics. They are the ambient medium in which electron beams travel outwards.

2. *Stochastic, fragmented energy release*: At the base of each fiber, at a random time, a random number of electrons is assumed to be accelerated, and to travel outwards.
3. *Bump-on-tail instability*: The particle distribution may eventually develop a hump, and primary Langmuir (L) waves are created (see e.g. Benz 1993).
4. *Strong turbulence*: Following Papadopoulos (1975), we assume the L-waves to grow to such a level that the beam-plasma system reaches a state of strong turbulence, where in the ambient plasma density-cavitons are formed (localized secondary Langmuir (L') waves, or solitons, through the oscillating two stream instability), and in turn secondary ion sound (s) waves are created (the primary ones are damped). The energy densities of the three different waves turn out to be stationary for a given growth rate of the primary L-waves (Vlahos and Rowland 1984; Rowland and Vlahos 1985).
5. *Non-linear wave-wave coupling* in the weakly turbulent plasma in-between the Langmuir clumps (which are very scarcely distributed) yields radio-emission at the local plasma frequency and its harmonic (random-phase wave-wave coupling, Papadopoulos and Freund 1979). The model spectrogram finally is the superposition of the emissions from all the fibers.

The model presented here is a continuation and improvement of the type III model of Vlahos and Raoult (1995). The modifications include: adding of harmonic radiation (with adequate spectrogram representation), allowing electron-populations of different types to be injected, consequent randomizing of exterior parameters, improving of the growth-rate estimate for the bump-on-tail instability, treating more thoroughly the three dimensional aspects of the problem, and a more realistic estimate of the energy loss of the beams.

All the numerical values for densities, spatial and temporal scales which will be given in the subsequent sections are chosen such that spectrograms which are close to observations in appearance are yielded, with the constraint, however, that these values are still in a physically reasonable range. We stress the fact that none of the parameters was directly fitted from the observations presented later, they merely were phenomenologically optimized.

2.2. The fibers

The n fibers are assumed to be static and isothermal, so that their density is barometric, and to be overdense compared to the surrounding coronal plasma by a random factor $\alpha^{(i)} \in [5, 100]$ (chosen uniformly at random), whence the density $n^{(i)}(z)$ in the i th fiber is

$$n^{(i)}(z) = \alpha^{(i)} n_0 e^{-z/H} \quad (1)$$

where z is measured along the axis of the fiber (else a magnetic term would have to appear). We assume $n_0 = 4.7 \cdot 10^8 \text{ cm}^{-3}$,

and a scale height $H = 1.9211 \cdot 10^9$ cm. The particle distribution function is a Maxwellian,

$$f_{amb}^{(i)}(z, v_z, t) = \frac{\alpha^{(i)} n_0 e^{-z/H}}{\sqrt{2\pi} v_{th,e}} e^{-\frac{1}{2} \left(\frac{v_z}{v_{th,e}} \right)^2} \quad (2)$$

The n fibers are independent of each other, they merely have the same temperature $T_e = 10^6$ K and consequently the same thermal electron speed, defined via $\frac{1}{2} m_e v_{th,e}^2 = \frac{1}{2} k_B T_e$. They are also assumed to have the same radius $d_0 = 2.0 \cdot 10^8$ cm at their base ($z = 0$), and to open upwards with a half opening angle $\theta = 5^\circ$. This angle influences the shape of the burst profiles as a function of frequency. With too large angles, the dilution of the beam (see Sect. 2.4) is so strong, that the emission is largest at the highest frequencies, decreases then and increases again towards lower frequencies. The chosen value of 5° is low enough, so that the emission increases with decreasing frequency, as it is in accordance with the observations.

2.3. The injected electrons

At the base of the i th fiber ($z = 0$) a hot population of electrons is injected with a density which is a random fraction $\beta^{(i)} \in [5 \cdot 10^{-8}, 5 \cdot 10^{-6}]$ of the ambient density $n^{(i)}(z)|_{z=0} = \alpha^{(i)} n_0$ (see Eq. 1). The injection takes place over a random height $L^{(i)} \in [2.0 \cdot 10^7 \text{ cm}, 2.0 \cdot 10^8 \text{ cm}]$ (centered at $z = 0$) and during a random time interval $\tau^{(i)} \in [0 \text{ sec}, 0.1 \text{ sec}]$. After all, the injected distribution is

$$f_{inj}^{(i)}(z, v, t) = \beta^{(i)} \alpha^{(i)} n_0 g(v_z) e^{-\left(\frac{z}{L^{(i)}}\right)^2} e^{-\left(\frac{t-t^{(i)}}{\tau^{(i)}}\right)^2} \quad (3)$$

centered around a random time $t^{(i)}$, which is chosen randomly as $t^{(i)} \in [0 \text{ sec}, n/5 \text{ sec}]$ so that on the average 5 beams per second are injected (n is the number of fibers, i.e. beams). The injected velocity distribution $g(v_z)$ is such that the corresponding distribution of the kinetic energies E is a power-law,

$$p_E(E = \epsilon) d\epsilon = \left(\frac{-\delta^{(i)} + 1}{E_2^{-\delta^{(i)}+1} - E_1^{-\delta^{(i)}+1}} \right) \epsilon^{-\delta^{(i)}} d\epsilon \quad (4)$$

with E_1 and E_2 the lower and upper energy cut-offs, respectively. This implies through $E = \frac{1}{2} m_e v_z^2$ that

$$g(v_z) = \left(\frac{-2\delta^{(i)} + 2}{v_2^{-2\delta^{(i)}+2} - v_1^{-2\delta^{(i)}+2}} \right) |v_z|^{-2\delta^{(i)}+1} \quad (5)$$

where $v_1 = \sqrt{2E_1/m_e}$ and $v_2 = \sqrt{2E_2/m_e}$, and where we have assumed $g(-|v_z|) = 0$. The cut-offs are chosen so that the injected particles can be considered as a hot tail to the ambient plasma: $3 v_{th,e} \leq v_z \leq c$ (c is the velocity of light). The power-law index $\delta^{(i)}$ varies randomly from fiber to fiber (i.e. from acceleration event to acceleration event) within the range $\delta^{(i)} \in [\delta_1, \delta_2] = [1.12, 1.80]$. This range is chosen according to the power-law indices of the empirical hard X-ray peak-flux distributions, as reported by Crosby et al. (1993).

2.4. Beam propagation

The distribution of the beam electrons evolves according to the one-dimensional Boltzmann equation

$$\frac{\partial f_{beam}^{(i)}}{\partial t} + v_z \frac{\partial f_{beam}^{(i)}}{\partial z} = -\nu_{e,e} f_{beam}^{(i)} + f_{inj}^{(i)} \quad (6)$$

where $\nu_{e,e} = 2.19 \cdot 10^{19} n^{(i)}(z)/v_z^3$ is the collision frequency for e-e-collisions. After solving this equation for $f_{beam}^{(i)}(z, v_z, t)$, we take the opening of the fibers (Sect. 2.2) into account in a simplified way, assuming that the beam particle density undergoes a dilution due to particle conservation. The total distribution function (beam plus ambient plasma) in the i th fiber therewith is

$$f^{(i)}(z, v_z, t) = \frac{1}{\left(1 + \frac{z}{d_0} \tan \theta\right)^2} f_{beam}^{(i)}(z, v_z, t) + f_{amb}^{(i)}(z, v_z, t) \quad (7)$$

(Note that the divergence of the field lines does not alter the distribution function of the ambient electrons, it is included in the barometric formula).

2.5. Wave generation

The electron distribution may develop a bump on the tail, i.e. a regime with positive slope, so that Langmuir waves with a growth rate

$$\gamma/\omega_{p,e} = \frac{\pi}{2} v_{max}^2 \frac{1}{n_{amb}} \frac{\partial f^{(i)}}{\partial v_z} \Big|_{v_z=\omega/k} \quad (8)$$

are generated (see e.g. Benz 1993). If a hump appears, then its beginning v_{beg} and its maximum v_{max} are determined, and the above growth rate is approximated as

$$\gamma/\omega_{p,e} = \frac{\pi}{2} v_{max}^2 \frac{1}{n_{amb}} \frac{f^{(i)}(v_{max}) - f^{(i)}(v_{beg})}{v_{max} - v_{beg}} \quad (9)$$

Papadopoulos (1975) has shown that in the low corona the conditions for strong turbulence are fulfilled. This does not necessarily hold anymore in the interplanetary space, where weak turbulence is most likely to occur (see Robinson (1997), who discusses electron beams at a distance 1 AU away from the Sun). Therefore, since we model type III bursts in the decimetric and metric range, we can assume the beam-plasma system to be in a strongly turbulent state. This implies that density cavitons are formed (solitons), the primary Langmuir waves are scattered away from resonance through the oscillating two-stream instability (and thereby the beam is stabilized), forming clumps of secondary Langmuir waves, and ion sound waves are created (Papadopoulos 1975; Rowland and Papadopoulos 1977). A detailed quantitative model for the energy densities in the different waves has been worked out by Vlahos and Rowland (1984) and Rowland and Vlahos (1985). They derived rate-equations for the wave-energy densities in the primary Langmuir waves (index L), the secondary Langmuir waves (index L'), and the ion

sound waves (index s). Solving these equations, it turns out that the energy densities reach a stationary state,

$$\begin{aligned} W_L &= 1 \cdot 10^{-5} n^{(i)}(z) k_B T_e \\ W_{L'} &= 7 \cdot 10^{-2} \frac{\gamma}{\omega_{p,e}} n^{(i)}(z) k_B T_e \\ W_s &= 3 \cdot 10^{-2} \frac{\gamma}{\omega_{p,e}} n^{(i)}(z) k_B T_e \end{aligned} \quad (10)$$

(in erg/cm^3), depending only on the linear growth-rate. The Langmuir clumps rule the energetics of the beam, they are, however, very scarce in space and time, and we may therefore assume that the electromagnetic emission stems from the weakly turbulent plasma in-between the Langmuir clumps (Eq. 10 actually describes the average wave-energy densities in the plasma, which is, with very localized and very short-living exceptions, in a weak turbulence state, according to Vlahos and Rowland 1984 and Rowland and Vlahos 1985). The electrostatic waves may coalesce and yield fundamental emission of electromagnetic (t) waves at the local plasma frequency $\nu_{p,e}$ with power

$$P_F^{(i)}(\nu = \nu_{p,e}) = 2 \Delta V 2\pi \nu_{p,e} 10^6 \tilde{W}_s \tilde{W}_{L'} \left(\frac{v_{max}}{c} \right)^2 \quad (11)$$

($L' + s \rightarrow t$; random phase-approximation, Papadopoulos and Freund 1979), and harmonic emission at the frequency $2\nu_{p,e}$ with power

$$P_H^{(i)}(\nu = 2\nu_{p,e}) = 0.4 \Delta V 2\pi \nu_{p,e} 10^6 \tilde{W}_{L'}^2 \left(\frac{v_{max}}{c} \right)^2 \quad (12)$$

($L' + L' \rightarrow t$), where the \tilde{W}_k are defined as $\tilde{W}_k = W_k / n^{(i)}(z) k_B T_e$ ($k = L, L', s$), and $\Delta V = 2 \frac{H}{\nu} d(z)^2 \pi$ is the size of the emitting volume ($d(z)$ is the radius of the fiber at height z). The power radiated by the i th fiber amounts to

$$P^{(i)}(\nu, t) = P_F^{(i)}(\nu, t) + P_H^{(i)}(\nu/2, t) \quad (13)$$

(the units are arbitrary).

2.6. Beam stopping condition: energy losses

The primary Langmuir waves have their energy at the expense of the kinetic energy of the beam (the secondary L' -waves and the s -waves in turn are fed by the primary L -waves) (Vlahos and Rowland 1984; Rowland and Vlahos 1985). In a stationary state, the region where the beam has passed through will be filled with waves, not uniformly, however, but the waves occur in localized, inhomogeneously distributed regions (Papadopoulos 1975; see also Lin et al. 1981). The filling factor of these clumps of Langmuir waves is small. We estimate the loss of energy of the beam at height z as

$$E_{beam,loss}^{(i)}(z) = r \int_{z=0}^z W_L d^3V \quad (14)$$

where the integration region is the axi-symmetric 3D-cone with radius d_0 at $z = 0$ and opening angle θ (see Sect. 2.2), and r is the filling factor. r is chosen randomly as $0.01 \leq r \leq 0.7$,

weighted, however, with the beam-energy in such a way that fast beams have higher filling factors. This takes into account the fact that high-energy beams are more stable, the enhanced non-linear effects (stronger Langmuir clumping) reduce their losses into waves. The beam in fiber i is stopped if

$$E_{beam,loss}^{(i)} = 0.3 E_{beam,inj}^{(i)} \quad (15)$$

with $E_{beam,inj}^{(i)}$ the initial kinetic energy of the accelerated particles. The alternative to this arbitrary beam-stop is to model the diffusive decay of the beam, which would give just a better description of a small part in the spectrogram, so that we may neglect it in the model.

We note that the filling factor influences how far a beam travels, i.e. what the bandwidth of a type III burst will be. The range we used for it was not derived from a fit to observations, but chosen ad-hoc to yield bursts of several hundred MHz bandwidth, on average.

2.7. Spectrograms

To generate model spectrograms (emitted flux as a function of frequency and time), the radio emission at the frequencies

$$\nu = 111.8 \text{ MHz}, 167.7 \text{ MHz}, \dots, 2012.5 \text{ MHz} \quad (16)$$

(i.e. with a step of 55.9 MHz) of all the n fibers is calculated and added (the step). Note that, for a given frequency ν , also the harmonic emission at $\nu_{p,e} = \nu/2$ has to be calculated, so that more frequencies are calculated than what enter the final spectrogram. Occasionally, due to this set-up, events with a bandwidth smaller than 55.9 MHz might not be seen, or possibly for some narrow-band emission the corresponding fundamental or harmonic might not be present in the spectrogram.

Computationally, we proceed as follows: For fiber i , at height z (which corresponds to a given local plasma-frequency ν), $f(z, \nu, t)$ at time t is calculated. This yields the contribution to the emission of fiber i at frequency ν and time t . This is repeated then for different times, afterwards for different frequencies, and finally the emissions from the different fibers are added. In Fig. 1, an example of a spectrogram generated by the model is shown.

3. Comparison of the model to data through peak-flux distributions

To judge the adequateness of the model, we compare the numerically generated spectrograms to observational data. The quantity of comparison shall be the peak-flux distributions, for which, in the spectrograms, a frequency is selected, the peaks are identified, the respective flux-values at the peaks are collected, and their histogram is computed.

For this purpose, a spectrogram containing the F- and H-emissions of 6000 fibers is generated with the model (a part out of this spectrogram corresponding to 200 seconds is the one shown in Fig. 1), and the frequencies 223.6, 670.8, 1118.0, and 1565.2 MHz were chosen to determine the peak-flux distribution at each of them. On the other hand, five type III events

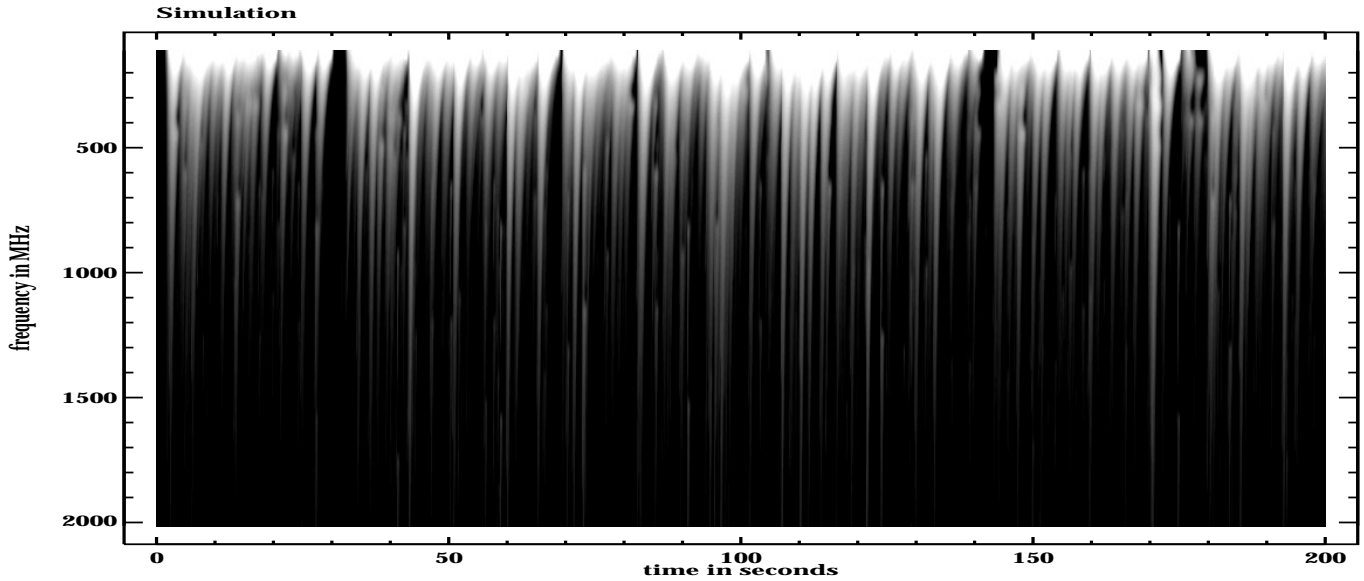


Fig. 1. 200 seconds of a spectrogram generated by the model, with time resolution 0.02 sec and frequency resolution 55.9 MHz. For a better representation of the spectrogram, a constant background is added to the radio fluxes, and the flux is logarithmized. The flux units are arbitrary.

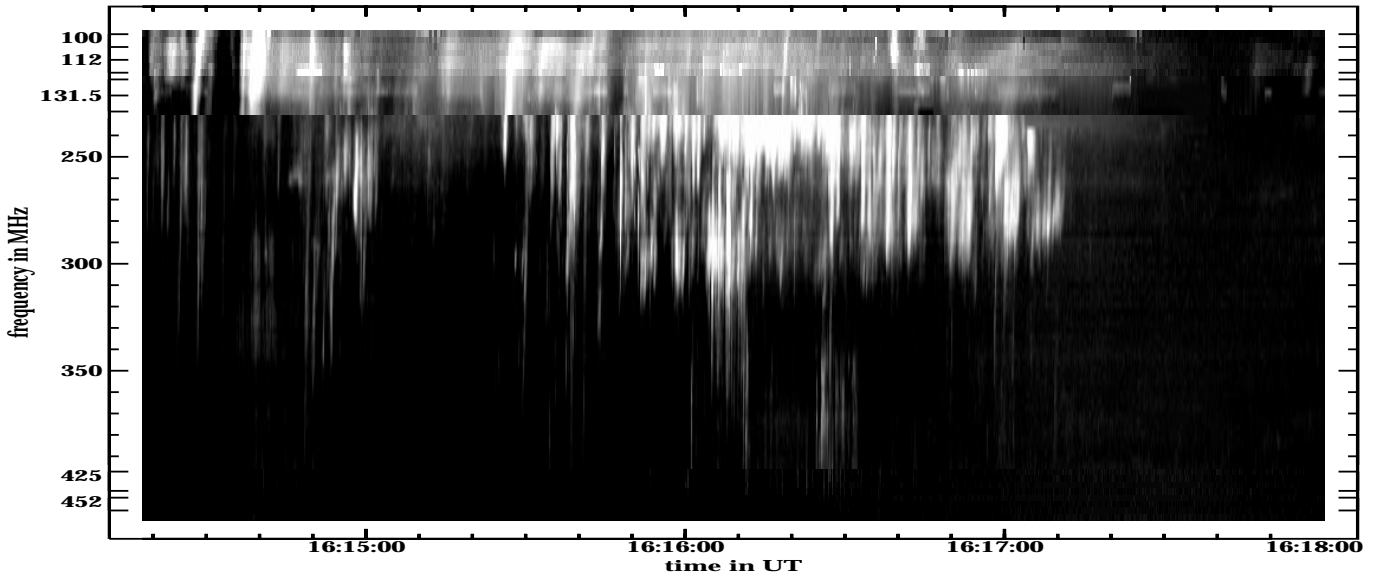


Fig. 2. Spectrogram of the type III event on 1980/06/27, 16:14:18 UT, observed by the ETH Zürich radio spectrometer (time resolution 0.1 sec, shown duration 200 sec).

observed by the ETH Zürich radio-spectrometer were analyzed (an example of a spectrogram is shown in Fig. 2), in which frequencies with relatively many peaks were selected, in order to have a reliable statistics. Since there is additive noise superimposed on the empirical data, it had to be visually checked whether a numerically detected peak is really a type III burst, or merely a fluctuation in noise.

3.1. Comparing the peak-flux histograms with the χ^2 -test

To quantify the comparison of the model histograms to the observational ones, i.e. to answer the question whether from a statistical point of view they can be considered as being generated

by the same process, the χ^2 -test is appropriate: Let $\{n_i\}$ denote the number of observed peak-fluxes in the i th of the totally n_{bin} bins of the histogram, so that consequently $\sum_{i=1}^{n_{bin}} n_i = n$ is the total number of observed peaks, and let m_i be the number of peaks from the model spectrograms in the very same bin (so that again $\sum_{i=1}^{n_{bin}} m_i = m$ is the total number of peaks from the model in all the bins). The test quantity is then defined as

$$\chi^2 = \sum_{i=1}^{n_{bin}} \frac{(\sqrt{\frac{m}{n}} n_i - \sqrt{\frac{n}{m}} m_i)^2}{n_i + m_i} \quad (17)$$

(see e.g. Press et al. 1992), which, if the two histograms are generated by the same process, follows a χ^2 -distribution with n_{bin}

degrees of freedom. The two distributions can be considered to be the same on a significance level of 95% if they differ less than a certain value $\chi_{95\%}^2$, which is taken from the χ^2 -distribution with n_{bin} degrees of freedom.

The result of comparing in this way all the observational data to the four different frequencies of the model is that four out of five observations can be considered compatible with the model, as is shown in Table 1: they have at least one frequency which behaves statistically in the same way as at least one of the frequencies of the model. Fig. 3 shows an example of a (normalized) empirical peak-flux distribution, together with the respective distributions of the four selected frequencies of the model, which all are compatible with the depicted observational distribution (see Table 1). As indicated in Table 1, in all cases we smoothed a minimum envelope (smoothed running minimum, corresponding to high-pass filtering) to the observational data and subtracted it. This is done since firstly the quiet emission of the Sun has to be subtracted for a comparison, and secondly, in four of the five events a time-varying background is present, which persists also after the type III burst emission has stopped and which therewith can unambiguously be identified as an additional emission, it is not just the effect of superposition of bursts close in time. Since the time-scale of this background is much larger than the one of the bursts, subtraction of a minimum envelope is adequate (the length of the running window is indicated in the tables). After all, the meaningful entries in Table 1 are those with a subtracted background.

The reason why we have not just compared equal frequencies of the model and the empirical data is that type III events have usually an individual highest starting frequency. The starting frequency of the model is around 2000 MHz, whereas in the five analyzed data sets it is lower. We might therefore adjust the starting frequency of the model, or else, and that is what we have done, compare different frequencies of the model to the data, to have beams in different stages of evolution (on a statistical average).

Concerning the spectrograms generated by the model as well as concerning the histogramming, a few remarks have to be made:

1: Since many of the beams injected in the model do not have enough energy to propagate very far, or to propagate at all, and since, above all at lower frequencies, the emission profiles of different beams merge, the number of bursts detected at a given frequency can be much less than the injected 6000 beams (see the respective entry in Table 2).

2: Generally, in a χ^2 -test, every model-parameter which is estimated from the data (those the model will be compared to) reduces the degrees of freedom by one, and if the model is forced to have the same total number of peaks as the observations do, the degrees of freedom are reduced by one, too (see e.g. Press et al. 1992). In our application, neither of the two constraints are fulfilled: first, the total number of peaks we have in the model is completely unrelated to the number of observational peaks. Second, none of the parameters of the model was estimated from the data-sets we compared the model to. They were chosen and optimized to yield spectrograms which

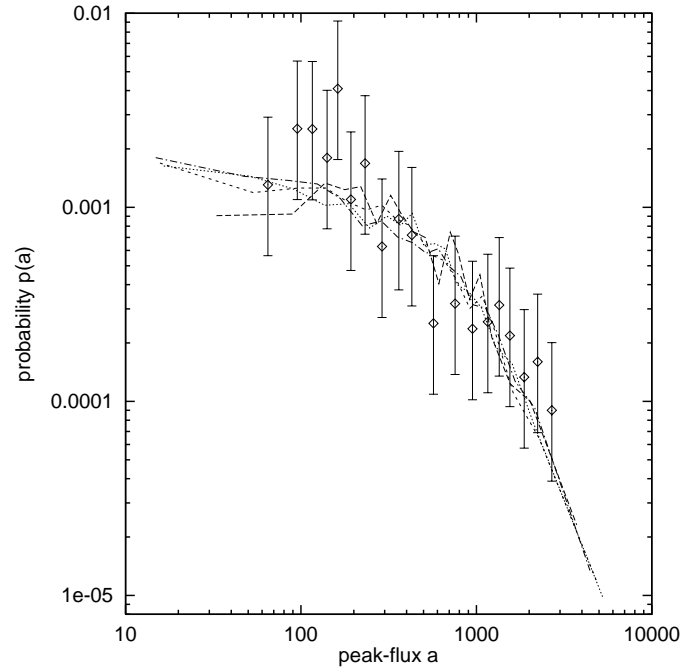


Fig. 3. Normalized histogram (probability density) of the peak-fluxes of the event observed on 1980/06/27, 16:14:18 UT, at 229 MHz (diamonds, with error bars; see also Fig. 2), together with the peak-flux distributions of the model at 223.6 MHz (dashed), 670.8 MHz (short dashes), 1118.0 MHz (dotted), and 1565.2 MHz (dash-dotted). For a better visualization, the histogram-values (probabilities) are depicted at the midpoints of the bins, and eventually connected with lines.

phenomenologically have some known properties of type III bursts, namely several hundred MHz bandwidth and less than 1 sec duration.

3: The flux-values of the model are in arbitrary units, so that, in order to make a comparison to observed data possible, we need a calibration factor for the model, which we determine as follows: we rescale the peak-fluxes of the model so that they have the same mean value as the empirical peak-fluxes of a considered event. Mostly then, the peak-fluxes from the model are in the same range as the empirical ones, and those which are outside we discard, the ones which are larger since according to the shape of the histograms (see Fig. 3) we may say that large amplitude events are rare and only seen in very long time series, the ones which are smaller assuming that the small amplitude events are not seen in the measurements since they are below the noise-level. That this omitted part of the model-distribution is relatively small can be seen from the example in Fig. 3, where the *complete* distributions from the model are shown (they are just cut for the χ^2 -test).

4: The number of bins used in the χ^2 -test influences slightly its outcome, causing that the χ^2 value of Eq. (17) fluctuates, so that the corresponding probabilities may change by a few percent. This seems crucial near the confidence level (95%). However, such fluctuations must be considered as the statistical fluctuations inherent to any statistical test. The more data are analyzed, the less important becomes the dependence on the number of

Table 1. Results of the χ^2 -test which compares the histograms of the peak-flux distributions of different observations of type III events to the ones of the model (Sect. 3.1). The treatment of the data (subtraction of a minimum envelope or original data) is indicated by stating the length of the running window. The applied significance level is 95%, and when reached indicated by 'compat.', otherwise a '—' is depicted. (The number of peaks for the model data are given in Table 2.)

event	envelope subtracted	number of peaks	model 223.6 MHz	model 670.8 MHz	model 1118.0 MHz	model 1565.2 MHz
80/06/27, 16:14:18						
106 Mhz	none	48	—	—	—	—
“	10 sec	“	compat.	compat.	compat.	compat.
229 Mhz	none	95	—	—	—	—
“	10 sec	“	compat.	compat.	compat.	—
“	4 sec	“	—	—	—	—
301 Mhz	none	96	—	—	—	—
“	10 sec	“	—	—	—	—
82/04/18, 05:37:56						
105 MHz	none	54	—	—	—	—
“	200 sec	“	—	—	—	—
241 MHz	none	70	—	—	—	—
“	200 sec	“	compat.	compat.	compat.	compat.
322 MHz	none	31	compat.	compat.	compat.	compat.
“	200 sec	“	compat.	compat.	compat.	compat.
82/04/16, 13:10:01						
229 MHz	none	51	—	—	—	—
“	10 sec	“	—	—	—	—
301MHz	none	32	—	compat.	—	—
“	10 sec	“	compat.	compat.	compat.	compat.
82/04/14, 06:04:14						
229 MHz	none	27	compat.	compat.	compat.	compat.
“	10 sec	“	compat.	compat.	compat.	compat.
80/04/28, 17:06:24						
382 MHz	none	44	—	—	—	—
“	10 sec	“	—	—	—	—

bins. The rule we followed to choose the number of bins was to have five peak-fluxes per bin, a compromise between having small errors in the histograms and retaining still a lot of information on the shape of the peak-flux distributions. Generally, we found that the outcome of the χ^2 -test is not influenced if we have $5 \leq n_{bin} \leq \min[n, m]/5$ (n and m are the total number of peaks in the two data-sets), except in some rare cases where the probabilities corresponding to the χ^2 value fluctuate between 90% and 99%, and where by chance a case is diagnosed to be negative instead of positive.

5: All-over, the bin-width varies from bin to bin in such a way that the number of data-points per bin is always the same.

6: In order to improve the statistics on the side of the observations, we made the combined peak-flux distribution of the peaks of the four frequencies in Table 1 which are 229 MHz or 241 MHz, all with the minimum envelope subtracted. The resulting histogram is not compatible with the model, its shape is near to a simple power-law. This kind of comparison, however, we consider to be questionable, since firstly the subtracted background is different in every of the four frequencies, and secondly equal frequencies do not imply that the type III bursts are in a similar stage of their temporal evolution.

3.2. Fitting curves to the peak-flux distributions

An alternative approach to compare the peak-flux distributions is to fit different curves to the histograms, and to see whether the parameters of these fits (e.g. power-law indices) are the same within statistical fluctuations for the model and the data (if the fits are adequate, at all).

The curves we fit are different forms of power-laws:

$$f(x) = \begin{cases} a(x-b)^c + d & \text{(a)} \\ a(x-b)^c & \text{(b)} \\ ax^c & \text{(c)} \end{cases} \quad (18)$$

The parameters a, b, c, d are numerically determined by the non-linear Levenberg-Marquardt method (Press et al. 1992). The adequateness of the fit is judged by the averaged deviations between the fit and the model (normalized by the errors in the data-points), which can be assumed to follow a χ^2 -distribution (with the degrees of freedom equal to n_{bin} minus the number of estimated parameters). A 95% significance level is demanded in order a fit to be accepted. The curves are fitted to the normalized probability distributions $p(a_i)$ of the peak-fluxes, defined as $p(a_i) := n_i / (n \Delta a_i)$, where n_i is again the number of peak-flux values in the i th bin, Δa_i is the width of the bin and a_i its

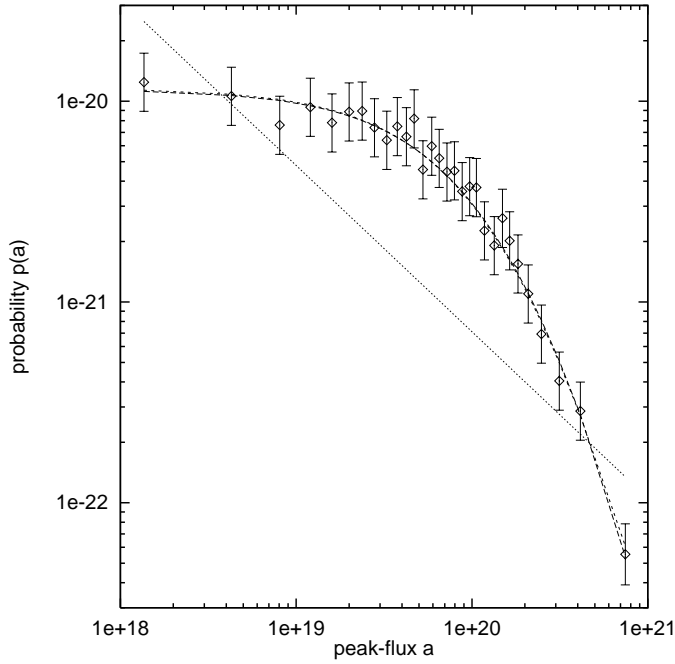


Fig. 4. Normalized histogram (probability density) of the peak-fluxes of the model at 670.8 MHz (diamonds, with error bars), together with the fits according to Eq. (18): $f(x) = a(x-b)^c + d$ (dashed), $f(x) = a(x-b)^c$ (short dashes), and $f(x) = ax^c$ (dotted). (Representation of the histograms as explained in Fig. 3.)

Table 2. For a realization of 6000 fibers, the result of a fit to the peak-flux distributions is listed for different frequencies and different fitted curves. The power-law index together with its error (determined by 100 bootstrap runs) is given if the fit is appropriate on a 95% significance level. A ‘—’ indicates that no significantly meaningful fit could be found. Throughout, histograms with 30 bins were used.

model	number of peaks	$a(x-b)^c + d$ $c :$	$a(x-b)^c$ $c :$	ax^c $c :$
223.6 Mhz	540	-3.3 ± 0.1	—	—
670.8 Mhz	987	-3.5 ± 0.4	-3.5 ± 0.5	—
1118.0 Mhz	1676	-3.6 ± 0.7	—	—
1565.2 Mhz	2017	-3.7 ± 1.3	-3.7 ± 0.5	—

midpoint. $p(a_i)$ is therewith the probability per unit-flux for a peak-flux of magnitude a_i to occur.

For the model spectrograms, all the peak-flux distributions could be described by the generalized power-law Eq. (18a), with indices around 3.5, the power-law Eq. (18b) was less successful, and the pure power-law fit (Eq. 18c) did not work at all (see Table 2; Fig. 4 shows an example of a model peak-flux probability-distribution together with the three fits). For the empirical data, all three power-law forms of Eq. (18) could be successfully fitted — since there are much less peaks than in the model-spectrograms, the errors in the probabilities $p(a_i)$ are larger, and the χ^2 -test becomes more tolerant. The estimated indices are given in Table 3, and Fig. 5 shows an example of a normalized peak-flux distribution together with the three fitted curves.

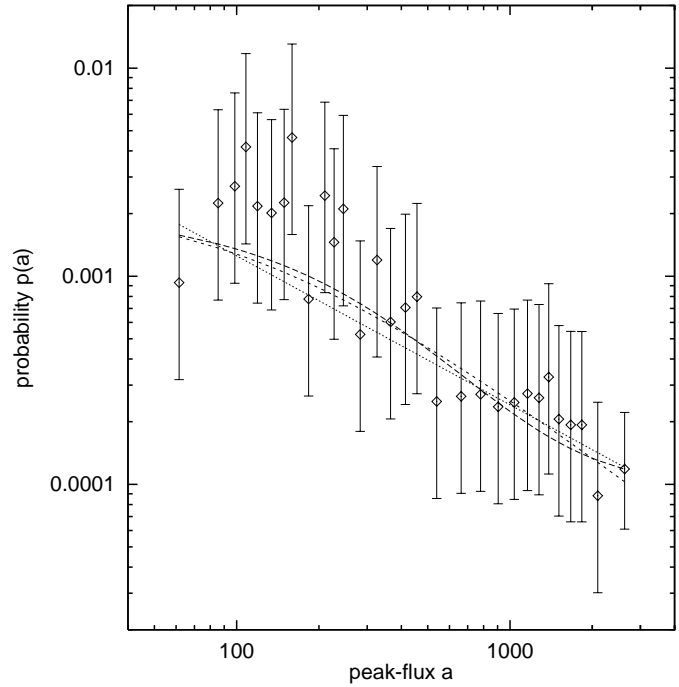


Fig. 5. Normalized histogram (probability density) of the peak-fluxes of the event observed on 1980/06/27, 16:14:18 UT, at 229 MHz (diamonds, with error bars; see also Fig. 2), together with the fits according to Eq. (18): $f(x) = a(x-b)^c + d$ (dashed), $f(x) = a(x-b)^c$ (short dashes), and $f(x) = ax^c$ (dotted). (Representation of the histograms as explained in Fig. 3.)

The case of interest is the generalized power-law fit of Eq. (18a), since it can be successfully fitted to the model and the observations, and therefore it can serve for a comparison. Unfortunately, the power-law indices estimated from the observed data scatter wildly for this fit. This scattering is due to the big errors in the estimates of the probabilities $p(a_i)$. It is therefore important to have a good estimate of the error of the estimated power-law indices. Due to non-linearity and largeness of errors, the usual Gaussian error propagation gives meaningless error estimates, the linearization done in this method is no longer valid. Therefore, the errors were determined by the bootstrap method, which works well also if non-linearities become important (see the Appendix for a description of the bootstrap method). For each error estimate, a sample of 100 surrogate data sets was used. It turns out that the errors for the empirical data are considerably large (Table 3). Assuming a Gaussian distribution for the errors of the power-law indices in Table 2 and 3, we see that the 3σ -intervals around the estimated indices of the model and the data mostly overlap. These intervals correspond to the respective 99.7% confidence intervals. Hence, in a statistical sense, the model and the data are compatible — therewith, the conclusion from the direct comparison of the histograms above (Sect. 3.1) is confirmed. However, it seems less stringent here, due the large errors of the observational power-law indices.

Remark 1: Concerning the influence of the number of bins onto the resulting power-law indices, it turned out that for a too small

Table 3. For different observations of type III events, the results of fits to the peak-flux distributions are listed. The power-law index together with its error (determined by 100 bootstrap runs) is given if the fit is adequate on a 95% significance level. A ‘—’ would indicate that the corresponding fit is statistically not significant. Histograms with 30 bins were used, throughout.

event	envelope subtracted	number of peaks	$a(x - b)^c + d$ $c :$	$a(x - b)^c$ $c :$	ax^c $c :$
80/06/27, 16:14:18					
106 MHz	none	48	-0.6 ± 3.4	-11.4 ± 3.9	-0.8 ± 1.2
“	10 sec	“	-12.6 ± 3.6	-2.6 ± 3.7	-1.0 ± 0.2
229 MHz	none	95	-0.5 ± 5.9	-2.5 ± 2.0	-1.0 ± 0.2
“	10 sec	“	-2.5 ± 5.1	-1.0 ± 0.3	-0.7 ± 0.2
“	4 sec	“	-7.7 ± 6.5	-1.0 ± 1.5	-0.7 ± 0.2
301 MHz	none	96	-15.3 ± 3.0	-7.8 ± 5.6	-1.4 ± 0.3
“	10 sec	“	-15.8 ± 4.6	-2.5 ± 6.4	-1.1 ± 0.2
82/04/18, 05:37:56					
105 MHz	none	54	-2.1 ± 3.1	-2.0 ± 0.3	-1.3 ± 0.1
“	200 sec	“	-2.1 ± 3.1	-2.0 ± 0.4	-1.2 ± 0.1
241 MHz	none	70	-4.4 ± 7.4	-1.3 ± 4.2	-1.5 ± 0.3
“	200 sec	“	-4.4 ± 7.5	-1.3 ± 4.2	-1.1 ± 0.2
322 MHz	none	31	-17.2 ± 6.6	-17.0 ± 5.1	-2.3 ± 1.5
“	200 sec	“	-17.2 ± 6.8	-17.0 ± 4.9	-1.5 ± 1.6
82/04/16, 13:10:01					
229 MHz	none	51	-0.6 ± 8.8	-2.9 ± 5.3	-2.1 ± 0.7
“	10 sec	“	-1.7 ± 7.2	-2.3 ± 5.9	-1.5 ± 0.3
301 MHz	none	32	-1.5 ± 7.0	-1.1 ± 3.0	-1.8 ± 0.4
“	10 sec	“	-1.5 ± 7.7	-1.0 ± 3.1	-1.3 ± 0.3
82/04/14, 06:04:14					
229 MHz	none	27	-0.5 ± 6.8	-15.3 ± 7.3	-1.1 ± 0.7
“	10 sec	“	-0.2 ± 6.7	-15.5 ± 7.5	-0.8 ± 0.6
80/04/28, 17:06:24					
382 MHz	none	44	-1.4 ± 6.3	-2.1 ± 4.7	-1.4 ± 0.2
“	10 sec	“	-3.2 ± 6.4	-1.6 ± 5.0	-1.2 ± 0.4

number of bins the estimates may depend on the latter, but they get stable if 30 or more bins are used, i.e. if a lot of information on the shape of the histogram is retained. We therefore used histograms with typically 30 bins, throughout.

Remark 2: The reason why we allow for a shift (cut-off) in the power-law fit (b in Eqs. 18a and 18b) is the following: If the true peaks $x^{(i)}$ are distributed with a power-law ($p_A(x) = ax^c$), and if there is an overall constant added, $\bar{x}^{(i)} = x^{(i)} + B_0$, e.g. the background radiation of the quiet Sun, then the transformed peaks are distributed as $p_{\bar{A}}(\bar{x}) = a(\bar{x} - B_0)^c$. The power-law index is still the same, but in a log-log plot one does not necessarily see a straight line anymore. This is the more important since when dealing with observations one has only a rough estimate of the background emission of the quiet Sun.

4. Discussion and conclusion

The model we introduced is a description of a randomly structured active region in which many local energy release events take place. The thereby accelerated particles escape through open fibers, develop a plasma-instability and create strong turbulence in the ambient medium. Wave-wave coupling finally leads to emission in the radio range.

The involved sub-processes are modeled in simplified ways — some more, some less —, since firstly there is so far only approximative theoretical knowledge on them, and secondly the needed boundary conditions are mostly unobservable. However, considering that type III events are the result of the interplay of many factors (structure of the active region, energy release mechanism, particle acceleration, propagation along fibers, plasma instability, turbulence), all with complex boundary conditions which moreover are different from burst to burst, one may expect that the details of the different sub-processes lose their significance, in the sense that a stochastic model is able to describe the type III phenomenon appropriately, it is not necessary to recur to a precise physical description of all the elements. In this spirit, different elements of the involved sub-processes were modeled as stochastic processes, and the highly complex initial and boundary conditions were represented by assuming different parameters to be random. This approach is presumably less promising if the interest would be in modeling a single electron beam (an isolated type III burst), where the questions would be to reproduce pulse-shapes, drift rates etc. The scope of this article, however, is to understand the statistical properties of entire type III events.

This argumentation finds its confirmation in the presented results: Concerning statistical properties of type III events, the

model is largely compatible with observations. Firstly, it yields peak-flux distributions which are compatible with four out of five events. Secondly, its time evolution is stochastic (by construction), as it should be to take the results of data-analysis of Isliker & Benz (1994) and Isliker (1996) into account.

It remains to remark that every statistical test applied to compare observations to models is rather tolerant, since the observational data intrinsically have a poor statistics, events with substantially more than 100 type III bursts are not seen. In other words, the discriminative power of the observations concerning the fine details of any model is very restricted, changing some elements in the model is likely not to spoil the compatibility with the observations — besides that, the single elements may anyway have only small influences on the statistics of the model spectrograms, as discussed above.

Under this proviso, we conclude that the observations are compatible with a model which assumes that: (i) the active region is highly inhomogeneous and randomly structured; (ii) the flare-particle acceleration-process is fragmented into a large number of sub-processes; (iii) the distribution of the accelerated particles is a random fraction of the ambient density, and of power-law form with a random index; and (iv) the fragmentary acceleration events occur randomly in time, i.e. the temporal structure of type III events is random, without any correlations between the individual bursts.

In future work, it will be investigated in how far different population-types for the injected electrons and different temporal organizations of the acceleration events may be excluded or accepted as other compatible explanations for type III bursts.

Acknowledgements. We thank A. Anastasiadis for many helpful discussions and comments. The work of H. Isliker was supported by a grant of the Swiss National Science Foundation (NF grant nr. 8220-046504), and the work of L. Vlahos was done in the frame of a PENED program of the Greek General Secretariat of Research and Technology. The construction of the radio spectrometers of ETH Zürich are financed by the Swiss National Science Foundation (grant nr. 20-46656.96).

Appendix A: error estimate by bootstrapping

To find the errors of the estimated parameters of the fitted curves in Sect. 3.2, there exist two methods, Gauss' error propagation and bootstrapping. In Gauss' error propagation, one represents the estimated parameters of e.g. $f(x) = a(x - b)^c + d$ as a function of the given data-points of the histograms, e.g. $c = h(\{x_1, y_1\}, \dots)$ (for conciseness of presentation, we write here $\{x_i, y_i\} := \{a_i, p(a_i)\}$ for the data-points). This relation is then linearized around the arguments which are subdued to an error, namely the y_i , whose errors $\sigma(y_i)$ are considered as small disturbances, and evaluation of the linearized formula yields the error of e.g. c as $\sigma^2(c) = \sum_j (\partial h / \partial y_j)^2 (\{x_1, y_1\}, \dots) \sigma^2(y_j)$. In order that this approach is successful, it is needed that the errors in the input data are mutually independent, and that they are sufficiently small so that the linearization is meaningful. The second assumption is hurt in our applications, and in general absurdly small values result for the errors (in some circumstances

even negative variances are yielded, due to numerics). Gauss' error propagation is therefore not applicable.

The bootstrap method is more general, no linearization is made: given are the pairs of data-points $\{x_i, y_i\}$, $i = 1, \dots, n_{bin}$, from which the parameters a, b, c, d are estimated. The idea of the bootstrap method is to resample the original data: one chooses randomly n_{bin} data-points $\{x_{i_k}, y_{i_k}\}$, $k = 1, \dots, n_{bin}$ out of the original set of data, whereby a data-point may occur several times (drawing with replacement). This procedure is repeated L times, and always the corresponding parameters $a^{(l)}, b^{(l)}, c^{(l)}, d^{(l)}$ are estimated, $l = 1, \dots, L$. The error of the original parameters, e.g. c , is then given by the standard deviation of the set of the $c^{(l)}$. (See e.g. Press et al. 1992.)

References

- Anastasiadis, A., Vlahos, L., Georgoulis, M.K., 1997, ApJ 489, 367
 Bastian, T.S., 1994, ApJ 426, 774
 Bastian, T.S., Benz, A.O., Gary, D.E., 1998, ARA&A (in press)
 Cairns, I.H., Robinson, P.A., 1995, ApJ 453, 959
 Benz, A.O., 1993, Plasma Astrophysics, Kluwer Academic Publishers, Dordrecht
 Benz, A.O., Aschwanden M.J., 1991, Characteristics of the impulsive phase of flares. In: Jackson, B.V., Machado, M.E., Svestka, Z.F. (eds.) Lecture Notes in Physics, IAU Coll. 133. Springer Verlag, Berlin
 Crosby, N.B., Aschwanden, M.J., Dennis, B.R., 1993, Sol. Phys. 143, 275
 Isliker, H., 1996, A&A 310, 672
 Isliker, H., Benz, A.O., 1994, A&A 285, 663
 Lin, R.P., Potter, D.W., Gurnett, D.A., Scarf, F.L., 1981, ApJ 251, 364
 Lu, T.L., Hamilton, R.J., 1991, ApJ 380, L89
 Mc Lean, D.J., Labrum, N.R., 1985, Solar Radiophysics, Cambridge University Press, Cambridge
 Melrose, D.B., 1980, Plasma Astrophysics: Nonthermal Processes in Diffuse and Magnetized Plasmas (2 volumes), Gordon and Breach Science Publishers, New York
 Oord, van den, G.H.J. (ed.), Fragmented Energy Release in Sun and Stars, proceedings, 1994, Space Sci. Rev. 68, 844
 Papadopoulos, K., 1975, Phys. Fluids 18, 1769
 Papadopoulos, K., Freund, H.P., 1979, Space Science Review 24, 511
 Press, W.H., Teukolsky, S.A., Vetterling, W.T., Flannery, B.P., 1992, Numerical Recipes, 2nd edition, Cambridge University Press, Cambridge
 Priest, E.R., 1996, New Developments in Magnetic Reconnection Theory. In: Tsinganos, K.C. (ed.), Solar and Astrophysical Magnetohydrodynamic Flows, NATO ASI Series, Series C: Mathematical and Physical Sciences 481, 171. Kluwer Academic Publishers, Dordrecht
 Robinson, P.A., 1997, Rev. mod. phys. 69, 507
 Rowland, H.L., Papadopoulos, K., 1977, Phys. Rev. Lett. 39, 1276
 Rowland, H.L., Vlahos, L., 1985, A&A 142, 219
 Vlahos, L., Georgoulis, M., Kluiving, R., Paschos, P., 1995, A&A 299, 897
 Vlahos, L., Raoult, A., 1995, A&A 296, 844
 Vlahos, L., Rowland, H.L., 1984, A&A 139, 263